JOURNAL OF PETROLOGY | VOLUME 36 | NUMBER 2 | PAGES 351–372 | 1995

MATTHEW W. NYMAN*, DAVID R. M. PATTISON AND EDWARD D. GHENT
DEPARTMENT OF GEOLOGY AND GEOPHYSICS, THE UNIVERSITY OF CALGARY, CALGARY, ALBERTA, CANADA T2N 1N4

Melt Extraction during Formation of K-Feldspar + Sillimanite Migmatites, West of Revelstoke, British Columbia

An exposure of sillimanite-rich, strongly deformed, stromatic, K-feldspar-bearing migmatites in the Monashee Terrane west of Revelstoke, British Columbia, has been examined to determine the process of migmatization and to evaluate whether the system was open or closed during leucosome formation. An anatectic origin for the migmatites is supported by: (1) the minimum melt composition of the leucosomes; (2) textures suggesting a fluid behavior of the leucosomes and local pegmatitic textures; and (3) P–T *estimates (720–820°C; 7·5–9 kbar) above vapor-absent melting conditions of muscovite + quartz.*

To establish whether melt was extracted or added during migmatization, measured volume percents of leucosome were compared with estimates of melt production modeled by muscovite + quartz dehydration melting. Quantitative estimates of volume percent of leucosome at present in the outcrop are between 20 and 30%. The amount of melt produced from the model muscovite dehydration melting reaction is constrained by measured modal percent of sillimanite (15–25%) in the outcrop and is dependent on modal proportion of muscovite in the unmelted protolith and the melt water content. Using a muscovite-rich protolith and a melt water content of 4 wt %, complete dehydration melting of muscovite results in a production of 54 vol % melt and 25 vol % sillmanite, indicating a melt loss of 29 vol %. A melt water content of 6 wt % results in production of 41 vol % melt and ~23 vol % sillimanite, indicating a melt loss of 16 vol %. Melt loss may have occurred by melt movement along foliation planes during flattening, during formation of shear bands or locally along subvertical fractures. Spatial proximity of the outcrop to the Monashee décollement suggests that thrusting was localized to zones of high melt production, which in turn facilitated melt migration.

KEY WORDS: *migmatites; British Columbia; Monashee Terrane; anatexis; melt extraction*

INTRODUCTION

A primary goal in the study of migmatites is to establish the processes by which high-grade metamorphic rocks become segregated into quartzofeldspathic layers (leucosome) and more mafic layers [melanosome and mesosome; for nomenclature see Ashworth (1985)]. Processes, in a closed system, which may cause migmatization include anatexis (partial melting) and subsolidus segregation. Open-system processes include intrusion of melts from nearby plutons, formation of veins from fluid infiltration at subsolidus conditions, or melting in response to introduction of fluid from an external source. Yardley (1978) discussed criteria for distinguishing between these possibilities. Evidence consistent with formation of migmatites by a melt-related process includes: (1) pressure and temperature estimates above the solidus for the rocks concerned; (2) more sodic plagioclase in leucosomes compared with mesosomes; (3) igneous textures within leucosomes (e.g. Vernon & Collins, 1988); and (4) where melt injection is suspected, proximity to plutonic rocks. Evidence consistent with a subsolidus process includes: (1) pressure and temperature estimates below the solidus of the rocks concerned; (2) textures and structures suggestive of infiltration and precipitation of leucosome along planes of weakness within the rock; and (3) plagioclase compositions more or less sodic in leucosomes compared with the host rocks. Ashworth (1985) outlined the dangers of relying on any single criterion to establish migmatization processes, especially where subsolidus processes such as diffusion and deformation may have altered mineral compositions or destroyed igneous textures.

Studies on whether leucosomes formed in an open

*Corresponding author. Present address: Department of Earth and Planetary Sciences, The University of New Mexico, Albuquerque, NM 87131, USA

or closed system have mainly used chemical and mass balance techniques (e.g. Dougan, 1979, 1981; Olsen, 1982, 1984). These studies hinge on the ability of the observer to identify, in the migmatized outcrop, both the unmigmatized precursor [paleosome or mesosome, using nomenclature of Ashworth (1985)] and the segregated portions of the rock, usually the leucosome and melanosome. Mass and chemical balance is then investigated assuming that leucosome + melanosome = paleosome. Persuasive evidence of internal derivation of leucosome and melanosome from paleosome is taken where this equality is statistically valid, whereas external processes are indicated when mass or chemical balance is not evident. The main difficulty in application of these techniques is the unequivocal identification of the unmigmatized protolith from which the leucosome and melanosome are derived. This may be especially problematic in strongly deformed migmatites where the mesosomes and paleosomes may have become separated, or in migmatites without distinct melanosomes.

Stromatic K-feldspar + sillimanite migmatites of the Monashee Terrane, British Columbia, are spectacularly exposed in road cuts southwest of Revelstoke. One outcrop over 100 m long and 20 m high provides an exceptional opportunity to investigate the mechanism of migmatization, evaluate, at the outcrop scale, whether migmatization occurred in an open or closed system, and investigate mechanisms for melt extraction during partial melting. An anatectic origin for these migmatites is supported by: (1) the presence of macroscopic and microscopic textures indicating the presence of a melt; (2) P–T estimates above muscovite vapor-absent melting; and (3) the presence of K-feldspar-free zones adjacent to some leucosomes, suggesting a local source for leucosome material. In contrast to other studies addressing open- vs closed-system migmatization, we have estimated the amount of leucosome within representative sections of the migmatite outcrop using photographs at various scales, and then compared these values with those calculated from inferred melting of the rock. The advantage of this approach is that it does not depend on identification of unmodified protolith or melanosome. This model additionally addresses the issue of open- vs closed-system behavior on an outcrop scale whereas many previous studies have relied mainly on investigation on a smaller scale.

REGIONAL GEOLOGY AND OUTCROP DESCRIPTION

The outcrop is located along the Trans-Canada Highway (Rte 1) ~3 km east of Three Valley Gap and 10 km west of Revelstoke, B.C. (Fig. 1). The rocks are part of the Monashee Terrane, a Mesozoic high-grade core complex within the Omineca Crystalline Belt of the Canadian Cordillera (Brown & Carr, 1990; Greenwood *et al.*, 1991). Uplift, synchronous with thrusting and Eocene brittle extension, has exposed the high-grade complex. The outcrop lies ~100 m below the Monashee décollement, a major Mesozoic (?) compressive fault zone (Brown & Carr, 1990).

Figure 2 is a series of line drawings, traced from photographs, of the outcrop. Figure 3 shows photographs of the outcrop, at various scales. The migmatites have a strong lineation defined by alignment of biotite + sillimanite aggregates, the long dimensions of quartz ribbons and the long dimensions of leucosomes. A more poorly developed planar fabric is defined by interlayering of mesosome and leucosomes. Asymmetric porphyroclasts of K-feldspar and garnet and shear bands which deform the foliation (Fig. 4b) indicate a shear component of the deformation, with tops to the north-northeast. Boudinage of leucosomes indicates a strong flattening component to the deformation.

K-feldspar + quartz-rich leucosomes range from centimeters to tens of meters in length and from a few millimeters to tens of centimeters in width. Thick leucosomes have a pegmatitic texture, are subparallel to the tectonic fabric and have an ellipsoidal shape with the long axis parallel to lineation.

At the west-southwest end of the outcrop there is a 1-m zone which is more strongly deformed and contains finely disseminated leucocratic material rather than discrete pods. At the east-northeast end of the exposure another zone of more intensely deformed rocks is present, in which the leucosomes are strongly deformed and the mesosome is fine grained, consisting predominantly of biotite + quartz ± garnet ± minor plagioclase. These two zones will hereafter be referred to as high-strain zones.

Cross-cutting pegmatitic K-feldspar + quartz veins (Fig. 3b and 3c) and a discordant pegmatitic pod (Fig. 2) also occur. Pegmatitic veins occur as 2–5 cm thick layers perpendicular to the foliation and clearly cut the fabric. At intersections with the layer-parallel leucosomes, the pegmatitic veins show continuous mineralogical and textural transition with the layer parallel leucosomes, with no evidence of cross-cutting relationships. These features suggest that the high-angle pegmatitic veins contained the same material as the stromatic leucosomes and were fluid. The pegmatitic pod shown in Fig. 2 has a similar mineralogy to the cross-cutting veins but occurs as a large undeformed mass within the high-strain zone at the north end of the exposure.

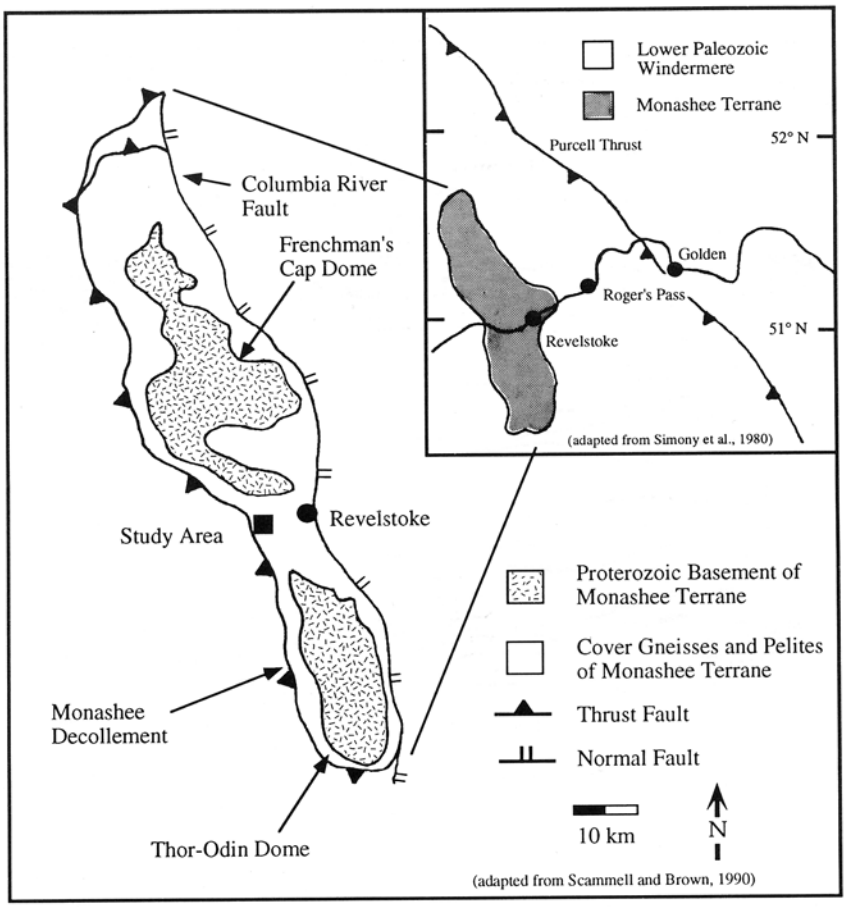

Fig. 1. Regional map of Monashee Terrane showing location of outcrop.

HAND-SPECIMEN DESCRIPTION

To observe the three-dimensional geometry of leucosomes, samples from the outcrop were cut parallel and perpendicular to lineation. All cut slabs were stained for feldspar, producing a strong yellow stain to K-feldspar and an off-white color to plagioclase.

Leucosomes can be separated into two general types. Type 1 leucosomes are stromatic with lensoid shapes and range in thickness from millimeter scale to tens of centimeters. Individual leucosome layers may show the full range of thickness variation (Figs 2, 3, and 4a and 4b). Type 1 leucosomes are commonly deformed by shear bands which either continue into the adjacent mesosome or curve into parallelism with the leucosome–mesosome boundary (Fig. 4b). In the rock adjacent to type 1 leucosomes there are 1–3 cm wide zones of biotite + sillimanite + garnet + quartz, devoid of K-feldspar (Fig. 4a). The width of these zones is proportional to the widths of the leucosomes. Several of the larger, centimeter-scale leucosomes contain wispy, garnet + biotite + sillimanite layers interpreted as thin screens of mesosome in a composite leucosome. In the high-strain zone at the north end of the outcrop, sillimanite is abundant in leucosomes and aligned parallel to the lineation in the adjacent mesosome.

Type 2 leucosome is characterized by two types of K-feldspar + quartz segregations. Type 2A leucosomes occur as narrow (<2 cm), finely disseminated, discontinuous layers intermixed with quartz + sillimanite + garnet $\pm$ plagioclase mesosome. Type 2B leucosomes occur as isolated grains of K-feldspar and quartz and are only found within pressure shadows of garnets. Type 2B leucosomes may be the result of preservation of type 1 leucosomes within pressure shadows of garnets during formation or, alternatively, represent local sites of leucosome generation and crystallization.

PETROGRAPHY OR MIGMATITES

The mineral assemblages and representative modes of mesosomes and leucosomes are shown in Table 1. Several samples which have millimeter-scale

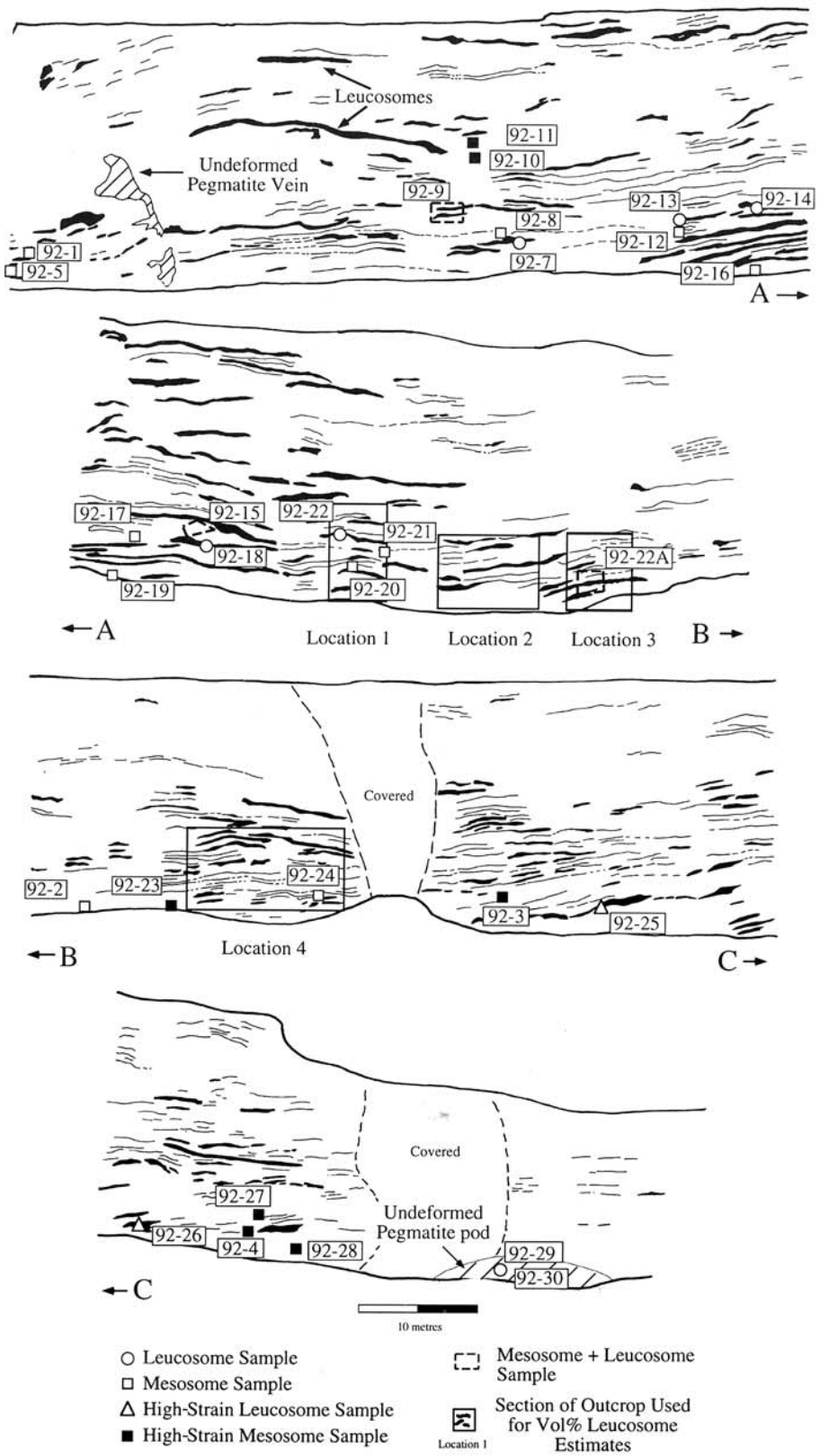

Fig. 2. Sketches of migmatite outcrop drawn from photographs. Letters with arrows indicate where the sketches connect. The top sketch is the southwestern end of the outcrop; the bottom sketch is the northeastern end.

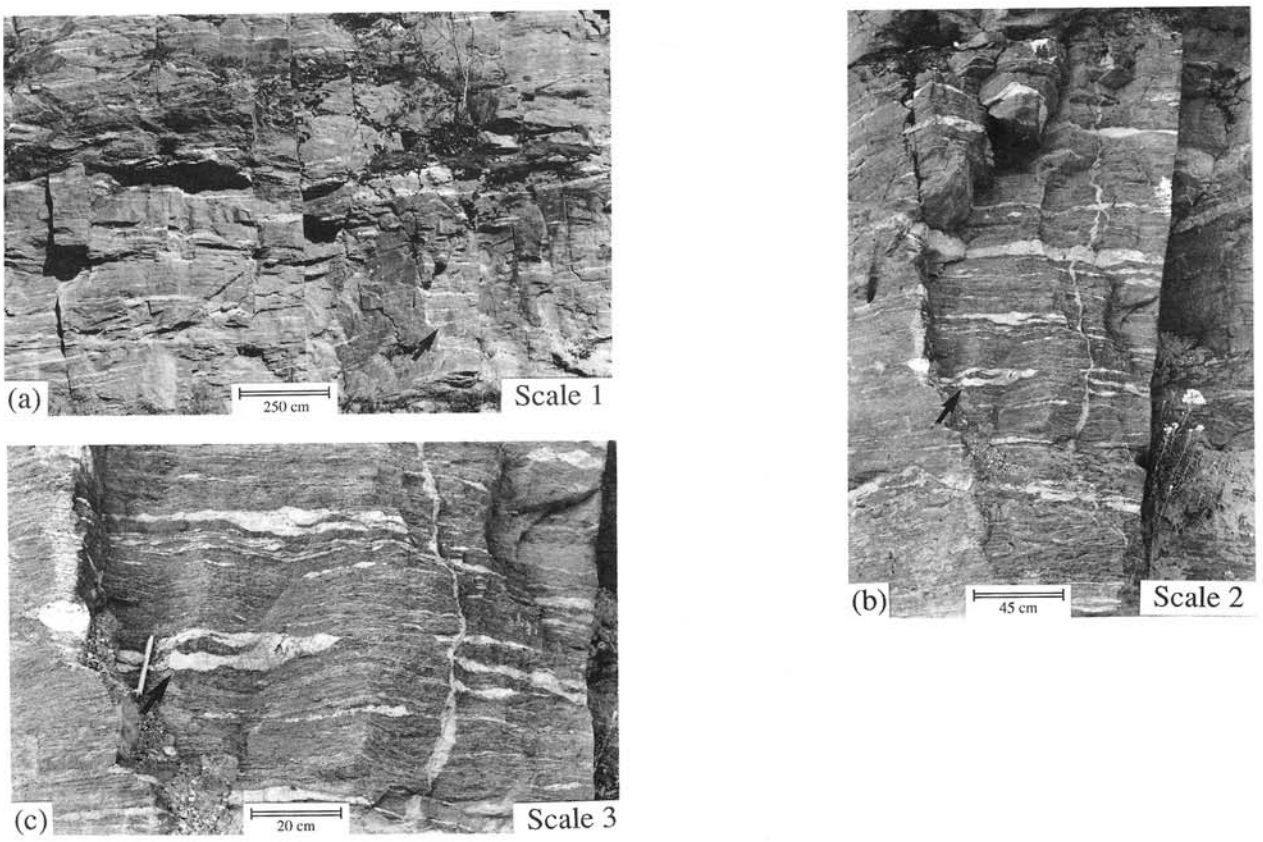

Fig. 3. Outcrop photographs from location 1 (see Fig. 2) taken from various distances. (Note the presence of K-feldspar + quartz dikes which cross-cut the stromatic leucosomes at a high angle.) Arrows indicate a stromatic leucosome observable at all scales.

leucosomes have been separated into leucosome, mesosome and garnet + sillimanite + biotite-rich melanosome (e.g. 9215C2).

Mesosome petrography

Mesosomes consist of garnet + biotite + sillimanite + quartz ± K-feldspar with minor amounts of rutile and/or ilmenite, graphite, and accessory apatite and zircon. Cordierite is a rare accessory in a few samples. Plagioclase was found in only four of the mesosome samples (Table 1). Mesosomes are generally well segregated into quartz-rich and garnet + biotite + sillimanite-rich layers interspersed with millimeter-scale K-feldspar + quartz segregations. K-feldspar free zones adjacent to leucosomes show greater segregation of sillimanite + biotite + garnet-rich layers and quartz-rich layers.

Garnet occurs as millimeter-scale idioblastic crystals and as ovoid crystals flattened in the plane of foliation. Most grains are strongly fractured, with several examples of disarticulated grains that can be reconstructed to their original shapes. The most strongly deformed garnets are nearly completely pseudomorphed by sillimanite + biotite. A local reaction texture suggesting consumption of garnet is evident where skeletal biotite, idiomorphic sillimanite and K-feldspar + quartz ± plagioclase are observed along margins of embayed garnet grains (Fig. 5a and 5b).

Sillimanite and biotite are intimately intergrown in all mesosome samples and form distinct layers. Within these layers, grain boundaries between sillimanite and biotite are straight with no evidence for biotite breakdown, suggesting that biotite + sillimanite are stable at the pressure and temperature conditions of the outcrop. Rarely, as discussed in a later section, there is microtextural evidence for incipient reaction of biotite within pressure shadows of garnet (Fig. 5), but the small-scale nature of these textures and the predominance of equilibrium textures between sillimanite + biotite + quartz argue in favor of overall stability of this assemblage. The importance of these inferences will be discussed in a later section.

Sillimanite is generally coarse grained but ranges in grain-size from fibrolite to crystals up to 3 mm in

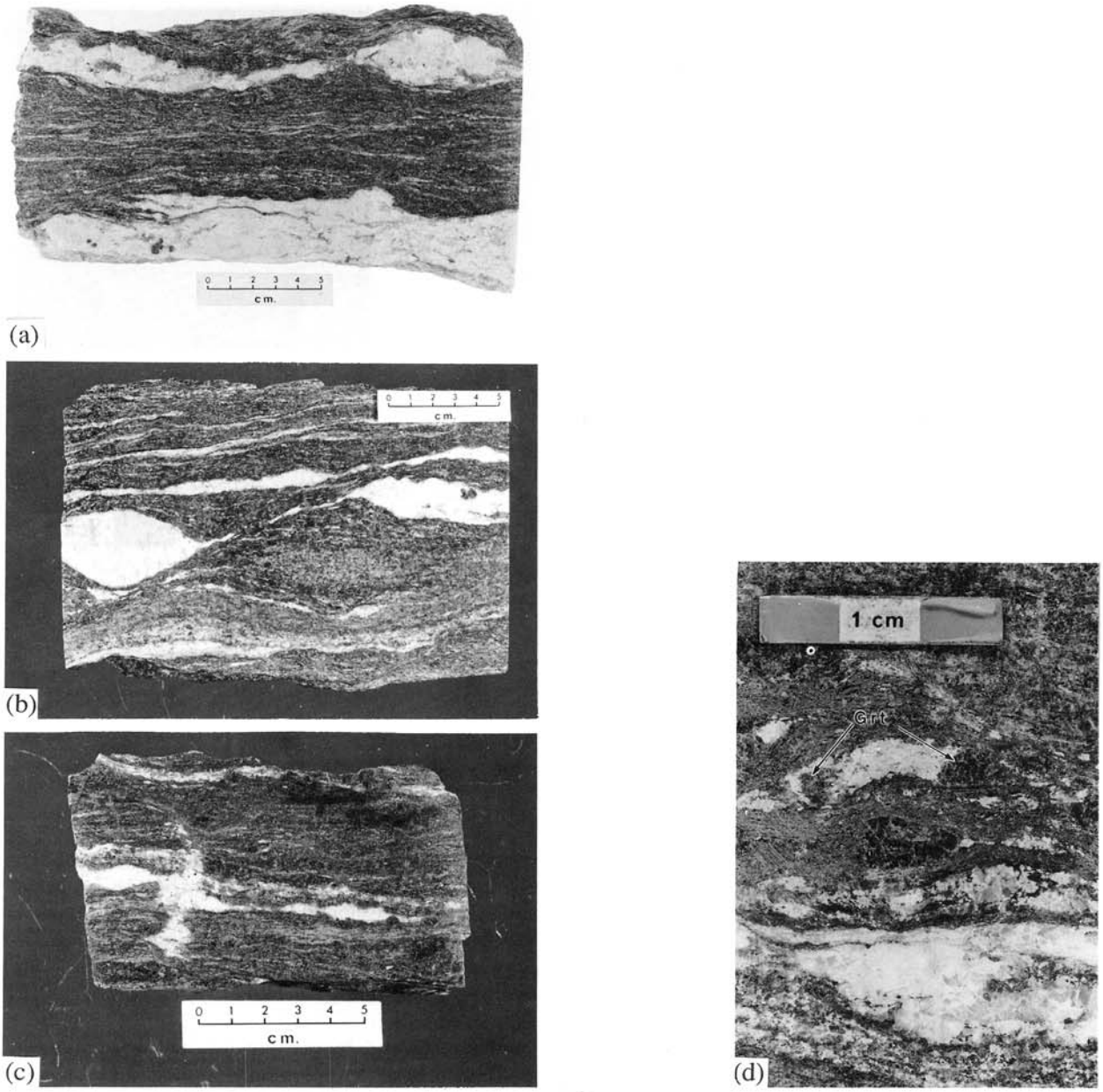

Fig. 4. Photographs of stained migmatite slabs. (a) Slab of migmatite showing typical variation in leucosome thickness. The bottom leucosome is bounded by ~2 cm thick K-feldspar-free zone. (b) Slab showing extreme thinning of a single leucosome layer along a sinistral shear band. The oval-shaped leucosome consists of a single K-feldspar grain. The more granular, darker zone above and below this layer is depleted in K-feldspar. (c) Migmatite slab showing a cross-cutting vein merging into a stromatic leucosome. The localization of the vein in a dilatant junction in a shear band suggests the vein was fluid. The cross-cutting leucosome has a weak fabric, suggesting later deformation following leucosome crystallization. (d) K-feldspar + quartz segregation between a garnet pull-apart.

width and 3 cm in length, with the long dimensions of the crystals generally aligned parallel to the tectonic fabric. Individual sillimanite needles may be strongly deformed, showing discrete kinks and boudinage. Fresh biotite has reddish brown pleochroism, consistent with the high measured Ti content. Biotite is commonly altered to chlorite intermixed with small rutile needles. Biotite is always altered adjacent to K-feldspar + quartz leucosomes and K-feldspar-bearing mesosome, whereas biotite isolated from K-feldspar is unaltered. This spatial relationship suggests that retrogression may be due to water released from the crystallizing leucosomes.

Rare cordierite typically occurs in mesosomes and leucosomes from high-strain zones. Cordierite, typically completely replaced by pinite, has two textural

Table 1: Modal amounts of minerals in selected leucosomes, melanosomes and mesosomes

Sample	*n*	Bt	Sil	Grt	Qtz	Kfs	G	Rt	Ilm	Kfs(1)	Qtz(1)
9215C3	1257	24·9	22·0	15·5	21·0	0·9	0·2	0·1	0·2	8·8	6·2
(whole)										(58·9)	(41·1)
9215C3	2447	21·8	20·6	17·8	29·0	9·8	0·1	tr	0·6	—	—
(meso)											
9215C1	2754	17·3	16·9	11·3	48·8	4·5	0·2	0·2	0·9	—	—
(meso)											
9215C2	457	12·9	12·5	8·3	66·1	—	—	0·2	tr	—	—
(meso)											
9215C2	900	2·2	0·4	—	31·6	65·6	tr	—	0·1	—	—
(leuco)											
9215C2	644	20·7	28·6	26·1	24·7	—	—	—	—	—	—
(melano)											
929D1	1654	26·9	24·7	6·1	35·4	6·4	0·1	0·1	0·2	—	—
(meso)											
923D	1093	25·6	16·7	20·6	18·9	0·5	0·1	0·1	0·1	10·9	6·3
(whole)										(63·3)	(36·7)
9215C6	1395	16·9	12·6	11·7	48·2	9·1	tr	0·2	1·3	—	—
(meso)											
922D	1594	16·1	21·2	5·3	41·8	14·6	0·6	0·1	0·3	—	—
(meso)											
921D	1704	33·0	18·8	19·1	28·1	0·8	0·2	tr	tr	9·8	5·5
(whole)										(62·7)	(35·1)
921P	1532	33·4	20·4	19·2	22·6	4·0	0·3	tr	tr	8·2	10·6
(whole)										(42·9)	(55·1)

Kfs(1): Kfs in millimeter-scale leucosomes within mesosome. Qtz(1): Qtz in millimeter-scale leucosomes within mesosome. Numbers in parentheses represent percentage of Kfs and Qtz in leucosome. 1D leucosome contains 2·24 modal % Ms. 1P leucosome contains 2·04 modal % Ms. Meso, mesosome; leuco, leucosome; melano, Bt + Grt + Sil-enriched layer; whole, mesosome + leucosome.

occurrences, as net-like material that includes biotite + K-feldspar + quartz inclusions, and as thin layers on the margins of embayed garnet grains adjacent to biotite. Garnet is typically absent in layers which contain the net-like cordierite.

In all samples quartz occurs as continuous ribbons parallel to the tectonic fabric, with incipient formation of subgrains and undulatory extinction. Rutile and/or ilmenite are found in all mesosome samples. Where found together, ilmenite rims rutile. Graphite occurs as flakes aligned parallel to the foliation and is more abundant in high-strain samples.

K-feldspar in mesosomes occurs as irregularly shaped grains with undulatory extinction, and is found within strain shadows of embayed, corroded garnet grains (Figs 4d and 5a) and in discontinuous, granular layers with quartz. Mesosome K-feldspar has similar petrographic characteristics to K-feldspar within leucosomes (see below), including spatial association with altered biotite and unaltered plates of biotite, and presence of dark intracrystalline inclusions. In mesosome samples from high-strain zones, K-feldspar has undergone significant grain-size reduction.

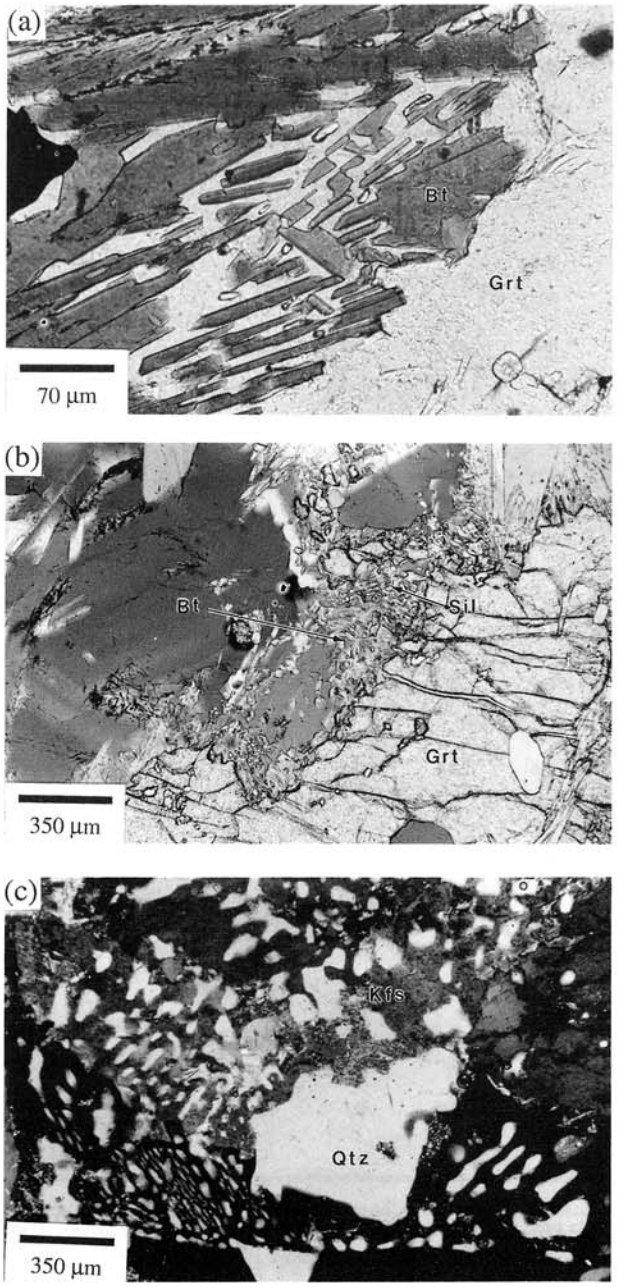

Fig. 5. Photomicrographs from migmatites. (a) Intergrown skeletal biotite and K-feldspar + quartz at the margin of an embayed garnet grain. (b) Similar texture to Fig. 4a except the biotite has a more wormy texture and occurs with sillimanite. (c) Granophyric texture from a leucosome.

Leucosome petrography

Representative examples of the modal mineralogy of the leucosomes are shown in Table 1. Leucosomes consist of K-feldspar + quartz with minor amounts of garnet, biotite and sillimanite, and rare muscovite and cordierite. Granophyric textures (Fig. 5c) are found in samples from several leucosomes and generally occur at the margins of large K-feldspar crystals. No plagioclase was found in any of the leucosomes, although some K-feldspars have sub-millimeter-sized albitic plagioclase inclusions aligned along late fractures. Biotite and garnet in leucosomes are partially replaced by chlorite, and sillimanite is typically altered to fine-grained muscovite. As with the alteration of biotite and garnet in the mesosome, this retrogression may be due to fluid released during crystallization of the leucosome. The similarity of the textures and compositions of sillimanite, biotite, garnet and muscovite with those in the mesosome suggests that they are mono- and poly-crystalline inclusions of mesosome in the leucosome, and did not crystallize from the leucosome.

K-feldspar grains within leucosomes show abundant evidence for subsolidus deformation, including undulatory extinction, kink bands oriented at high angles to the foliation and subgrain development. Quartz within leucosomes occurs as ribbons and irregular intergrowths with K-feldspar. Quartz ribbons wrap around large K-feldspar grains and leucosomes.

MINERAL CHEMISTRY

Analytical techniques

Mineral analyses were collected using a nine-channel ARL SEMQ electron microprobe at The University of Calgary, using silicate and oxide standards. Operating procedures and methods of calculation of detection limit and precision have been described by Nicholls & Stout (1988). Data were reduced using a Bence & Albee (1968) correction using an off-line computer program modified from Nicholls *et al.* (1977). Analyses were recalculated to cations number using spreadsheet programs, with garnet based on 12, biotite on 11, and feldspars on 8 oxygens. Representative analyses are shown in Table 2.

Biotites in the matrices of mesosomes and leucosomes are indistinguishable, except for a few analyses of a green biotite found in some leucosomes. Skeletal biotite grains in garnet pressure shadows have the same composition as matrix biotites. Biotite inclusions within garnets have slightly lower Ti contents than matrix biotites.

Biotite compositions are uniform throughout individual samples, although there is some variation between samples. Between samples, Fe/(Fe + Mg) ratios vary from 0·40 to 0·54, with an associated increase in Ti content of 0·13–0·26 cations. Cl and F contents are $<0{\cdot}5$ wt % and 0·2 wt %, respectively.

Garnet compositions in leucosomes and mesosomes

*Table 2: Representative microprobe analyses of garnet, biotite and feldspars**

	Garnet			Biotite			K-feldspar	K-feldspar	Plagioclase
Sample	921	922	923	921	922	923	922	923	923
SiO_2	37·92	38·68	38·72	35·66	35·83	36·83	64·75	63·62	57·43
Al_2O_3	21·27	21·54	21·92	17·41	18·52	19·04	18·69	19·01	27·94
TiO_2	0·01	0·00	0·02	4·12	2·89	2·41	—	—	—
FeO	34·01	34·07	28·85	20·21	18·62	15·10	0·21	0·08	0·01
MnO	0·20	0·13	0·47	0·01	0·01	0·03	—	—	—
MgO	6·86	5·68	7·32	10·14	10·05	12·59	0·01	0·00	0·00
CaO	0·44	0·54	2·47	0·01	0·01	0·03	0·02	0·05	9·31
Na_2O	—	—	—	0·22	0·16	0·11	1·10	1·53	6·78
K_2O	—	—	—	8·43	9·29	9·73	15·11	13·87	0·20
Cl	—	—	—	0·54	0·86	0·43	—	—	—
Total	100·71	100·64	99·77	96·74	96·23	96·29	100·25	100·10	101·69
Si	2·98	3·03	3·01	2·69	2·69	2·72	2·98	2·96	2·54
Al	1·97	1·99	2·01	1·51	1·64	1·66	1·02	1·04	1·46
Ti	0·00	0·00	0·00	0·26	0·16	0·13	—	—	—
Fe	2·23	2·23	1·88	1·30	1·17	0·93	0·01	0·00	0·00
Mn	0·01	0·01	0·03	0·00	0·00	0·00	—	—	—
Mg	0·80	0·66	0·85	1·11	1·22	1·39	0·00	0·00	0·00
Ca	0·04	0·05	0·21	0·00	0·00	0·00	0·00	0·00	0·44
Na	—	—	—	0·03	0·02	0·02	0·10	0·14	0·58
K	—	—	—	0·84	0·89	0·92	0·89	0·82	0·01
Total	8·04	7·97	7·98	6·87	6·88	6·85	5·00	5·00	5·03
Fe/(Fe + Mg)	0·74	0·77	0·69	0·54	0·49	0·40	—	—	—

*Cations for garnet, biotite and feldspars recalculated on the basis of 12 O^{2-}, 11 O^{2-} and 8 O^{2-}, respectively.

are indistinguishable, being in the range Alm 58–67, Pyr 23–35, Sps 0–1, Grs 1–7. Compositional profiles across a single garnet adjacent to biotite show an enrichment of almandine and spessartine and depletion of pyrope and grossular components at the outer 200–300 μm of the crystal. This zoning pattern is typical of all garnets that are in immediate contact with biotite. Compositional profiles at grain margins are generally flat where garnet is adjacent to quartz or feldspar. Based on the antipathetic variation in Fe and Mg only where garnet is in contact with biotite, the compositional variation is interpreted as late-stage diffusion-controlled Fe–Mg exchange with biotite (Tracy, 1982).

K-feldspars contain between 9 and 19 mol % albite component and only minor anorthite. Plagioclase compositions were only measured in two samples and have an average composition of An_{56}.

EVIDENCE FOR A LOCAL ANATECTIC ORIGIN FOR THE MIGMATITES

Mineralogic and textural evidence

The leucosomes have eutectic (K-feldspar + quartz) mineralogy for the binary K-feldspar + quartz system. The absence of plagioclase in the leucosomes is matched by the general absence of plagioclase in the mesosome, suggesting a local origin of the leucosomes. Internal derivation of the leucosomes is further suggested by the presence of K-feldspar-free zones around large leucosomes.

Several textures suggest that before crystallization the leucosome had fluid properties and was fluid during deformation. The similarity in composition and textures of the cross-cutting veins and stromatic leucosomes, and the lack of any textural discontinuities between the two, suggests that the stromatic leucosomes may have been fluid, possibly being the sources for the cross-cutting veins. Figure 4c shows a shear band along which leucosome material cross-cuts the tectonic fabric, suggestive of injection into a dilatant gap in the shear band. Dilation may have been facilitated by increases in pore pressure and decrease in effective normal stress during melt accumulation within the shear band.

Additional evidence for fluid behavior of leucosome is shown in Fig. 4d, which shows K-feldspar + quartz leucosome between pulled-apart garnet fragments. During fracturing and separation of the garnet, leucosome material must have formed or migrated into the gaps. Garnets associated with these features typically have strongly embayed margins and may be partially replaced by biotite ± sillimanite ± quartz intergrowths. The similarity between biotite compositions in the replacement textures and matrix suggests that garnet replacement occurred at or near peak metamorphic conditions.

As a result of the strong deformation that accompanied and followed migmatization, microtextures associated with leucosome crystallization have largely been overprinted by subsolidus deformation textures. Rarely, undeformed portions of the migmatites preserve textures suggestive of leucosome crystallization from a magmatic fluid. Granophyric textures (Fig. 5c) are found within leucosomes preserved in the pressure shadows of large K-feldspar crystals. Granophyric texture is a common feature in granites and is thought to be due to simultaneous crystallization of quartz and K-feldspar from a melt (e.g. Mehnert, 1968).

Figure 5a shows randomly oriented, idioblastic biotite plates in a K-feldspar + quartz matrix, in a garnet pressure shadow. Figure 5b shows another example of this texture within a garnet pressure shadow where biotite has a wormy texture intergrown with K-feldspar and small, idioblastic sillimanite crystals. The garnet margins are severely embayed, and remnant garnet fragments occur within the biotite + sillimanite + quartz + K-feldspar mosaic in Fig. 5b. These textures suggest that garnet is being consumed, producing biotite + sillimanite which show a delicate static, skeletal texture in a K-feldspar + quartz matrix, suggestive of crystallization from a melt. A possible model reaction to explain this texture is

$$\text{Grt} + \text{melt} = \text{Bt} + \text{Sil} + \text{Qtz} \qquad (1)$$

[mineral abbreviations from Kretz (1983)] the reverse of inferred prograde melting reactions (see below). We infer that reaction between garnet and melt occurred as the rocks cooled with fluid released from the crystallizing leucosome to produce biotite. Similar textures in other migmatites have also been interpreted as indicating the presence of a melt (Kenah & Hollister, 1983; Ashworth & McLellan, 1985; Pattison & Harte, 1988; Vernon & Collins, 1988).

P–T estimates and phase equilibria

P–T estimates were calculated for several mesosome samples using individual matrix biotites surrounded by K-feldspar + quartz and core analyses of garnets away from marginal zones showing evidence of Fe–Mg exchange. These estimates were determined using the program TWQ (Berman, 1988, 1991) and are constrained by the intersection between the temperature-sensitive garnet–biotite equilibrium and the pressure-sensitive net transfer equilibria

$$\text{Alm} + \text{Rut} = \text{Ilm} + \text{Al-Silicate} + \text{Qtz} \qquad (2)$$

and

$$\text{Grs} + \text{Al-Silicate} + \text{Qtz} = \text{An}. \qquad (3)$$

The solution models used in the calculation are listed in Table 3.

Temperature estimates range from 720 to 1081°C (Table 3). The wide range is probably a reflection of disequilibrium in some of the samples, exemplified by textural features such as the retrograde zoning of the garnet and reaction textures within garnet pressure shadows. The two high values (924 and 1081°C) are inconsistent with the biotite + sillimanite + quartz mineralogy as, at these temperatures, biotite + sillimanite should have ceased to be stable together, contrary to the observed equilibrium textures

Table 3: Pressure and temperature estimates from mesosomes

Sample:	921	921	921	922	923	923
P–T ID:	921·1	921·2	921·3	922	923·1	923·2
Grt–Bt	920	820	790	750	1080	810
T estimate (°C)						
Alm–Rt–Als–Ilm	820	750	750	760	—	—
P estimate (MPa)						
Alm–Als–An	—	—	—	—	1400	900
P estimate (MPa)						

Sample 921 contains Ilm with no Rut, which means pressures are maxima. Pressures and temperatures were estimated using the program TWQ (Berman, 1991). The following solution models were used: garnet—Berman (1990); feldspars—Fuhrman & Lindsley (1988); biotite—McMullin *et al.* (1991).

within mesosomes (Le Breton & Thompson, 1988; Vielzeuf & Holloway, 1988; Peterson & Newton, 1989; Vielzeuf & Clemens, 1992). Estimates of pressure also show a significant range, varying between 750 and 900 MPa, with one unreasonably extreme value of 14 kbar (Table 3). Thus, the P–T conditions are estimated to have been somewhere in the range 720–820°C and 750–900 MPa.

Figure 6 is a P–T plot of experimental data showing some key reactions for pelites at this metamorphic grade, along with P–T estimates from this study. All of the P–T estimates fall on or above the dehydration–melting curve of muscovite in the KASH system, which is a good analog for these generally plagioclase-free migmatites. All of the P–T estimates fall above invariant point II formed by the intersection of the subsolidus muscovite dehydration reaction (3), the water-saturated melting curve of muscovite + K-feldspar + quartz (4) and the muscovite + quartz vapor-absent melting curve (3). This indicates that, in the absence of an infiltrating low-a_{H_2O} fluid, reaction of muscovite + quartz to sillimanite + K-feldspar must have been accompanied by formation of a melt phase rather than a free vapor phase.

MODELING OF MELT VOLUME GENERATION

Below we evaluate whether the amount of leucosome measured in representative sections of the outcrop is consistent with volumes of melt expected to have been produced in the rocks. We assume that the major melt- and sillimanite-producing reaction is muscovite vapor-absent melting:

$$\text{Ms} + \text{Qtz} = \text{Sil} + \text{Kfs} + \text{Melt}. \qquad (4)$$

This assumption is supported by (1) the presence of abundant muscovite in low-grade equivalent rocks; (2) the absence of primary muscovite within the outcrop; and (3) P–T estimates which indicate metamorphic conditions above muscovite vapor-absent melting. Rare petrographic evidence for minor melt production by biotite dehydration melting is preserved in garnet pressure shadows; however, the predominance of equilibrium textures between biotite + sillimanite + quartz indicates minimal reaction between these phases.

Melt volume estimates from muscovite vapor-absent melting are constrained by the measured modal abundance of sillimanite in the outcrop. If the system was closed during migmatization, the calculated amounts of melt and sillimanite produced by reaction (4) should have been within the range of measured modal abundances of sillimanite and leucosome. Deviation between measured and calculated values would indicate an open system. The possibility of sillimanite formation downgrade of the muscovite + quartz vapor-absent reaction is incorporated in the modeling. Wet melting of a muscovite-bearing minimum melt assemblage of K-feldspar + albite + quartz may have occurred at lower metamorphic grade but, in the absence of water infiltration during melting, melt volumes for this reaction will be low, owing to the low porosities of high-grade metamorphic rocks, which will inhibit

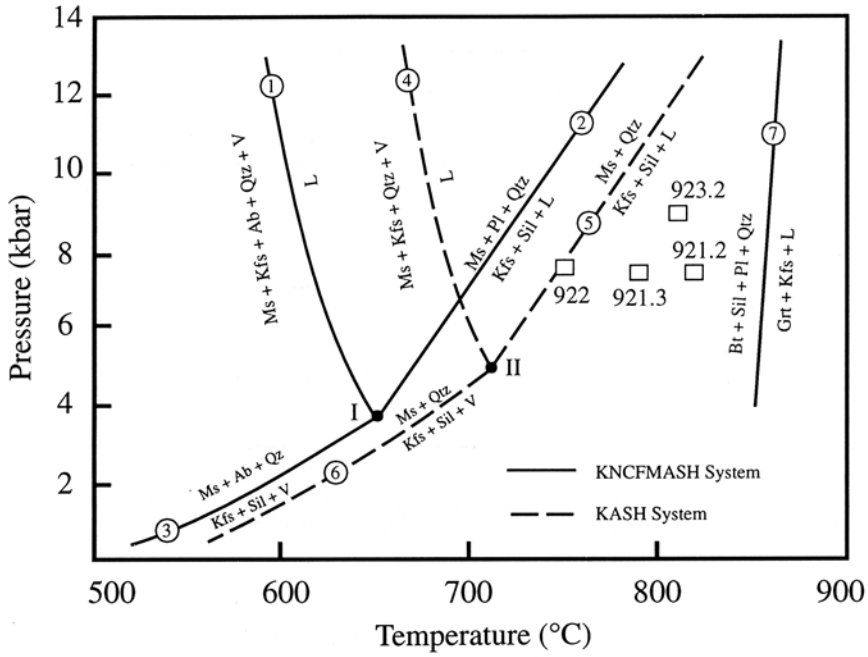

Fig. 6. *P–T* diagram showing the location of phase equilibria and pressure and temperature estimates from mesosome samples. The numbers 922, 923.3, 921.2 and 921.3 refer to sample numbers used in *P–T* calculations. The positions of the reactions were taken from the following sources: 1, Thompson & Tracy (1979); 2, Peto (1976); 3, Thompson & Algor (1977); 4, Vielzeuf & Holloway (1988); 5, Större (1972); 6, Chatterjee & Johannes (1974); 7, Vielzeuf & Holloway (1988). The invariant points I and II are from Thompson & Algor (1977).

large-scale fluid infiltration (Thompson, 1983; Tracy, 1986; Clemens & Vielzeuf, 1987).

Estimates of leucosome volumes

Estimates for the volume percent leucosome in the outcrop were obtained by tracing sections of the outcrop from photographs, taken at various scales (Fig. 3), and coloring the leucosomes black. The sketches were scanned to produce computer bitmap files of the images and, by using an image analysis program and high-resolution color monitor, the proportions of black and white pixels were counted to quantify the amounts of leucosome and mesosome, respectively. To take account of the fact that leucosomes occur at different scales (tens of centimeters to <1 mm), three scales were analyzed (Fig. 3 and Table 4). The amount of mesosome measured at scale 1 represents the new whole-rock volume at scale 2, and so on down to scale 3. The amount of leucosome at each scale was adjusted by multiplying the amount of leucosome by the percentage of mesosome from the previous scale (Table 4). For instance, at location 1 the volume of mesosome and leucosome is 92·19% and 7·81%, respectively (Fig. 2 and Table 4). For scale 2 at location 1, 7·81% of the whole rock has already been counted as leucosome at scale 1. Therefore, both leucosome and mesosome at scale 2 must be decreased by a factor of 0·92 (1·0 − 0·078) to account for the leucosome that was measured at scale 1. Leucosomes which already had been measured at higher scales were not re-counted at lower scales. The total amount of leucosome was determined by adding the amounts of leucosome measured at each scale. Inclusion of these three scales into the volume calculations covers the full range of leucosomes except for very finely disseminated K-feldspar in the mesosome at the smallest scale. Modal amounts of fine-grained K-feldspar within the mesosome range from 0 to 14%, with an average of ~5%. Therefore, cumulative measured volumes of leucosome were increased by 5% to account for this fine-grained K-feldspar + quartz. The results of the volume estimates are shown in Table 4. The volume percent of leucosome ranges from 22 to 31, averaging 28 vol % leucosome.

Modal abundance of sillimanite

Modal abundances of sillimanite in mesosomes are shown in Table 1. The normal range of modal sillimanite is 15–25 modal %, with a few samples containing as much as 28 modal % sillimanite; the average is 20%.

Table 4: Results of leucosome volume estimates

	% White = mesosome	% Black* = leucosome
Location 1		
Scale 1	92·19	7·81
Scale 2	97·15 × 0·92 = 89·56	2·85×0·92 = 2·63
Scale 3	84·79 × 0·895 = 77·3	15·21 × 0·895 = 13·62
Total leucosome		24·05 + 5 = 29·05
Location 2		
Scale 1	86·50	13·50
Scale 2	92·60 × 0·865 = 80·52	7·40 × 0·865 = 6·41
Total leucosome		19·91 + 5 = 24·91
Location 3		
Scale 1	82·34	17·66
Scale 2	89·69 × 0·823 = 71·35	10·31 × 0·823 = 8·49
Total leucosome		26·14 + 5 = 31·14
Location 4		
Scale 1	92·52	7·48
Scale 2	89·78 × 0·925 = 83·09	10·22 × 0 ·925 = 9·46
Total leucosome		16·94 + 5 = 21·94

*Black refers to color of pixels used in digital image analysis.

Protolith composition: Al-silicate from staurolite breakdown

As the volume of melt produced from reaction (4) is limited to the amount of sillimanite produced in the same reaction, it is essential to assess possible production of sillimanite from lower-grade reactions. Sillimanite could not have formed by a subsolidus reaction

$$Ms + Qtz = Sil + Kfs + V \qquad (5)$$

because P–T estimates lie above invariant point II in Fig. 6. However, some sillimanite may nevertheless have formed at lower grade by other subsolidus reactions, in particular the disappearance of staurolite. A representative reaction stoichiometry for staurolite breakdown is

$$0{\cdot}13\ St + 0{\cdot}07\ Ms + 0{\cdot}48\ Qtz = 1{\cdot}0\ Sil + 0{\cdot}06\ Bt + 0{\cdot}16\ Grt + 0{\cdot}27\ H_2O \qquad (6)$$

(see the Appendix and Table A2 for parameters used to calculate the balanced reaction). The above coefficients are similar to those of the staurolite-out reaction in the petrogenetic grid of Spear & Cheney (1989). Mineral densities were used to convert the above coefficients to mineral volumes. Results of volume calculations for the amount of Al-silicate produced during this reaction are shown in Fig. 7 and indicate that ~10% more staurolite is dissolved than sillimanite produced. Therefore, in a rock containing 10 modal % staurolite, ~9 modal % Al-silicate would be produced during the disappearance of staurolite.

To estimate the amount of staurolite, and therefore the amount of Al-silicate produced by this reaction, we compiled the modal abundances of staurolite and Al-silicate for world-wide occurrences of pelites at or near the staurolite-out isograd (Table A1). The range of staurolite contents is from trace amounts up to 20 modal %; however, only 8 samples out of 103 have >10% staurolite. Al-silicate (kyanite and/or sillimanite) abundances range from

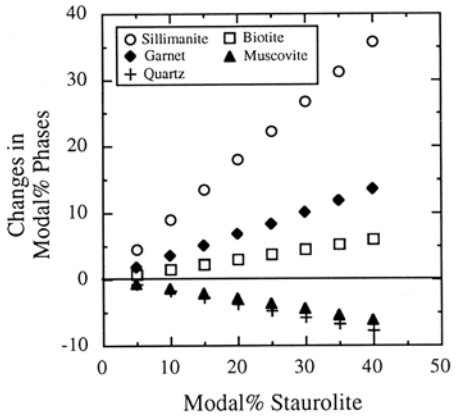

Fig. 7. Plot of modal changes of minerals as a function of amount of staurolite at the staurolite-out reaction. The reaction consumes muscovite, staurolite and quartz and produces sillimanite, garnet, biotite and water.

trace amounts to 31 modal %, with only five samples of 44 containing >5%, of which 4 also have ⩽2·0 modal % of staurolite (Chinner, 1960). Total amounts of staurolite + Al-silicate for the rocks compiled in Table A1 range from 6·5 to 10, with an average of 7·6. We have chosen the maximum of this range for the modal percentage of sillimanite present in the rocks after staurolite breakdown and before muscovite vapor-absent melting which will result in the most conservative estimates of melt production during muscovite dehydration melting. Biotite and garnet are also assumed to have formed at lower grade, the latter in part as a result of reaction (6).

On the basis of this analysis, we have used the following modal abundances as a starting composition for a rock undergoing muscovite-vapor-absent melting: 50% muscovite, 20% quartz, 10% sillimanite, 10% garnet and 10% biotite. The high modal percentage of muscovite and relatively low percentage of biotite is consistent with several samples examined from lower-grade equivalent pelites in the Mica Creek area of British Columbia (Robbins, 1976; sample DR-222). Modal analysis of a single kyanite-zone sample from the Mica Creek area reveals the following mineral abundances: biotite 2·1%, muscovite 54·8%, kyanite 1·1%, garnet 7·6%, quartz 33·2%, staurolite 0·59%, tourmaline 0·20%, opaques 0·32% ($n = 2534$). Also, as will be shown below, our results show that, in the absence of significant melt production by biotite dehydration melting as indicated by the equilibrium textures between biotite + sillimanite + quartz, the high modal percentage of muscovite is required to produce the amount of leucosome and sillimanite measured from the outcrop.

Influence of melt water content on calculated melt volumes

The model parameters used to calculate variation in volume percentage of phases and melt production during muscovite vapor-absent melting are outlined in the Appendix (Tables A3 and A4). Factors which affect the volume of melt produced during vapor-absent melting include the volume percentage of hydrates (muscovite) in the starting rock, the temperature and pressure interval over which melting occurs, and the water content of the melts (Clemens & Vielzeuf, 1987; Le Breton & Thompson, 1988). The melt water content additionally affects the physical properties of the melt.

There is no consensus on water contents of undersaturated melts produced from vapor-absent melting of muscovite. In a compilation of water contents of intermediate and silicic igneous rocks inferred to have crystallized from undersaturated melts, Clemens (1984) reported water contents ranging from <1 up to ~7 wt %, depending on magma composition, depth of magma generation, type of melting reaction and the amount of differentiation. In general, magmas generated at higher pressure have greater water contents. Clemens & Wall (1981) and Miller (1985) reported melt water content of ⩾8 wt % for conditions of muscovite vapor-absent melting at 4–10 kbar and ⩽700°C. Clemens & Vielzeuf (1987) used values of ~10 wt % for melts, from muscovite vapor-absent melting at 5 kbar and 12 wt % at 10 kbar, based on Burnham's model for albite melt–H_2O interaction.

Estimates of melt water content for the P–T conditions estimated in this study were made using Burnham's (1979) activity model for the albite–H_2O system and Nicholls' (1980) model for water contents of melts of different compositions. Application of Burnham's model requires an estimate of the activity of water. Using the program TWQ (Berman, 1988, 1991), estimates of water activity range from 0·50 to 0·70 for the estimated P–T conditions, which translates into ~9 wt % water for an albite melt using the Burnham model.

The thermodynamic model of Nicholls (1980) is based on experimentally measured water contents of a variety of melt compositions. From these relationships melt water contents for a variety of magma compositions can be calculated, on the basis of the P–T conditions and activity of water (a_{H_2O}). Using the equation of Haar for conditions of 800°C and 7·5 kbar and an activity of 0·60 the Nicholls equation predicts a melt water content of ~3 wt % for a melt composition of $Or_{55}Qtz_{45}$, the latter being a good model for the observed leucosome mineralogy. This

value is relatively insensitive to changes in a_{H_2O} and never exceeds 4 wt% for reasonable changes in values of activity.

Several workers have questioned whether Burnham's model is realistic physically and whether the model of the albite–H_2O system is applicable to more complex melt compositions (Stolper, 1982; Clemens & Vielzeuf, 1987; Navrotsky, 1987). The results using the Burnham model generally yield calculated water contents which are higher than experimentally determined values (Clemens & Vielzeuf, 1987). In contrast, the value of ~3 wt% water from Nicholls' model is below most other published estimates, although it is the middle of the range compiled by Clemens (1984). To cover the range of estimated water contents, we modeled the reaction for the following melt water contents: 12, 9, 6 and 4 wt%.

Results of modeling

Tables A3 and A4 show the parameters used to calculate the model results shown in Figs 8 and 9. The muscovite composition is from Ghent (1975) and the K-feldspar composition is the mean of K-feldspar grains in the leucosomes. Sillimanite and quartz are assumed to be pure. The melt compositions and molecular weights were calculated using the measured K-feldspar composition and a ratio of 60:40 K-feldspar to quartz, the latter being the mean modal ratio of K-feldspar to quartz in the leucosomes. The anhydrous molecular weights of the melt were calculated on the basis of 10 oxygens following the method of Waters (1988).

Variations in the leucosome and mineral volumes as a function of reaction progress were calculated using the values in Table A3 and the reaction coefficients in Table A4. To monitor the volume changes the following steps were used: (1) volume percent muscovite was decreased by 10%; (2) the resulting volume changes in the other phases were calculated; (3) these values were renormalized to 100. The calculations were continued until muscovite was exhausted. To construct Fig. 9, melt was removed once its volume exceeded 25% (the average observed volume of leucosome in the outcrop), with the remaining material renormalized to 100.

Variation in volume percent mineral phases and melt as a function of reaction progress was monitored by modal decrease of muscovite during vapor-absent melting. The results are shown in Fig. 8 for the four values of melt water content. In all cases, volume changes in garnet and biotite were <2% and have been omitted for clarity.

Closed system

For a closed system (constant volume) at low melt water contents (4 and 6 wt%) there is a relatively small modal increase in the amount of sillimanite (6–8%) during complete vapor-absent melting of the muscovite-rich pelite (Fig. 8a and 8b). There is little to no overlap between the modeled and observed volume percent leucosome (mean 25%; range 20–30%) and modal sillimanite (mean 20%; range 15–25%). In fact, the calculated volume percent melt (40–50%) produced with complete dehydration melting of muscovite far exceeds the observed volume percent leucosome. Dehydration melting of only 20–30 vol% muscovite does produce the range of observed volume percent leucosome but does not reproduce the observed amount of sillimanite.

With increasing melt water content (Fig. 8c and 8d) greater amounts of sillimanite are produced for the same extent of muscovite vapor-absent melting and there is greater overlap between calculated and observed volume percent melt and sillimanite. However, even with the most extreme values for melt water content (12 wt%) and vapor-absent melting of all the muscovite, the constant-volume model fails to produce the observed mean modal percent sillimanite (20%). Also, at melt water contents of 9 and 12 wt%, 14–17 vol% solid K-feldspar is produced, which is inconsistent with the observed average of 5 modal % K-feldspar within mesosomes.

It is difficult to determine whether isolated K-feldspar in the mesosome was produced as solid reaction products or crystallized from a melt that did not segregate into a discrete leucosome. Fine-grained K-feldspar in the mesosome has several textural similarities to leucosome K-feldspar, suggesting that it may represent small leucosomes that did not segregate. If the small (5%) modal percent of K-feldspar noted in mesosome represents solid K-feldspar, a low melt water content is indicated. Assuming that all of the K-feldspar is part of unsegregated leucosome, then the model melt volume in Fig. 8 should be increased by some factor to account for K-feldspar produced. However, increasing the melt volume by this factor would increase the discrepancy between observed and calculated quantities of melt + K-feldspar and sillimanite. To be conservative in the ensuing discussion, solid K-feldspar produced by muscovite vapor-absent melting is not included in estimates of the melt volume.

Open system

In contrast to the constant-volume models, it is possible that melt may have been extracted from the system, resulting in a relative increase in the modal

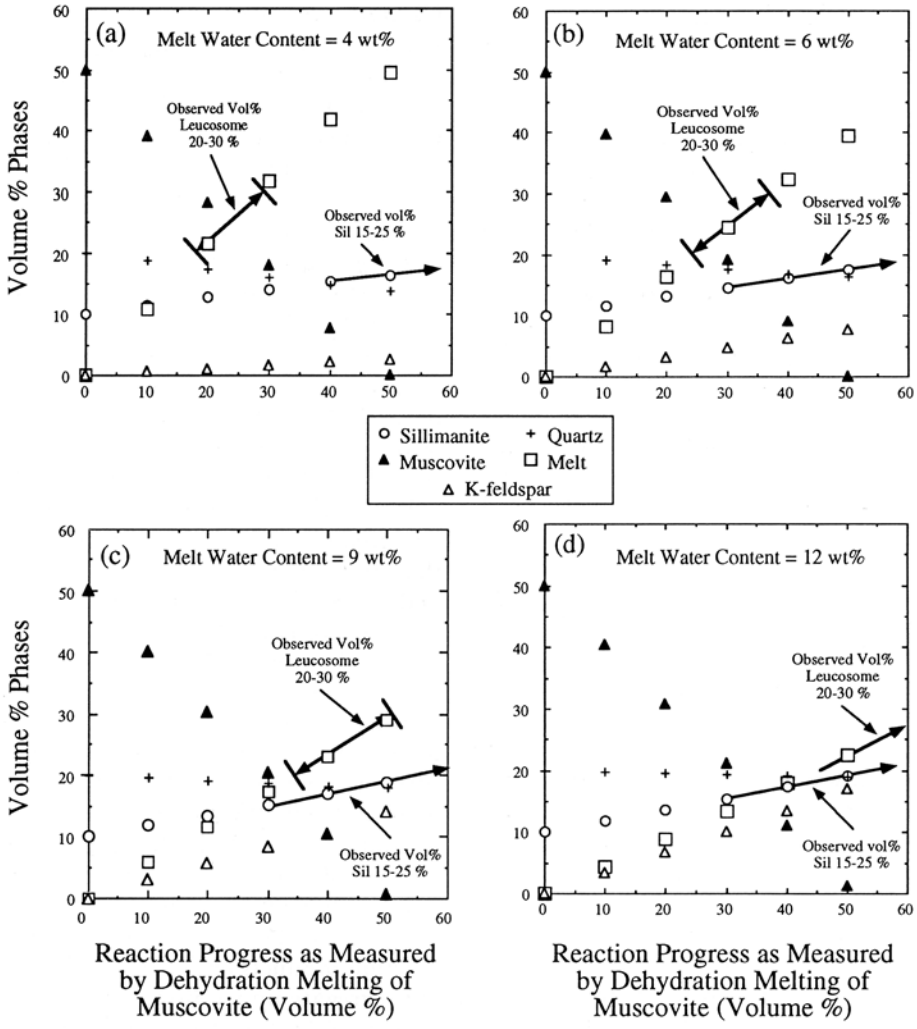

Fig. 8. Plots of modal variations during muscovite dehydration melting in a closed system as a function of changes in the modal abundance of muscovite. The double arrow shows the range of measured volume percent of leucosome in the outcrop. The single arrow shows the range of modal percent sillimanite in the mesosome. The different diagrams are for the four melt water contents discussed in the text.

amount of sillimanite and other phases in the remaining rock. Results of calculations assuming that any melt in excess of 25 vol % (the mean leucosome volume in the outcrop) was lost from the system are shown in Fig. 9. For a melt water content of 4 wt %, and maintenance of a melt volume of 25%, complete vapor-absent melting of muscovite results in a total melt production of 54 vol %, indicating a cumulative melt loss of 29% (Fig. 9a). This melt loss results in a relative increase in modal amount of sillimanite to 25%. These results are very close to the measured volume percentage of sillimanite and leucosome in the outcrop. Also, in this model ~5 vol % of solid K-feldspar is produced, consistent with the observed amount of K-feldspar in mesosomes. At a slightly higher melt water content of 6 wt %, cumulative melt loss of 16 vol % from a total melt production of 41 vol % results, but the modal proportion of sillimanite only reaches ~20% and up to 10% solid K-feldspar is produced. The model with 9 wt % water results in a very small melt loss of ~4 vol % with an increase in modal sillimanite to ~19 vol % and ~15 vol % solid K-feldspar. For a melt water content of 12 wt %, the volume of melt produced never exceeds ~22 vol %, and sillimanite volumes are <20%.

DISCUSSION

Melt volume produced from muscovite vapor-absent melting

Melt volumes produced from vapor-absent melting are controlled primarily by the water content of the melt and the modal abundance of the hydrous

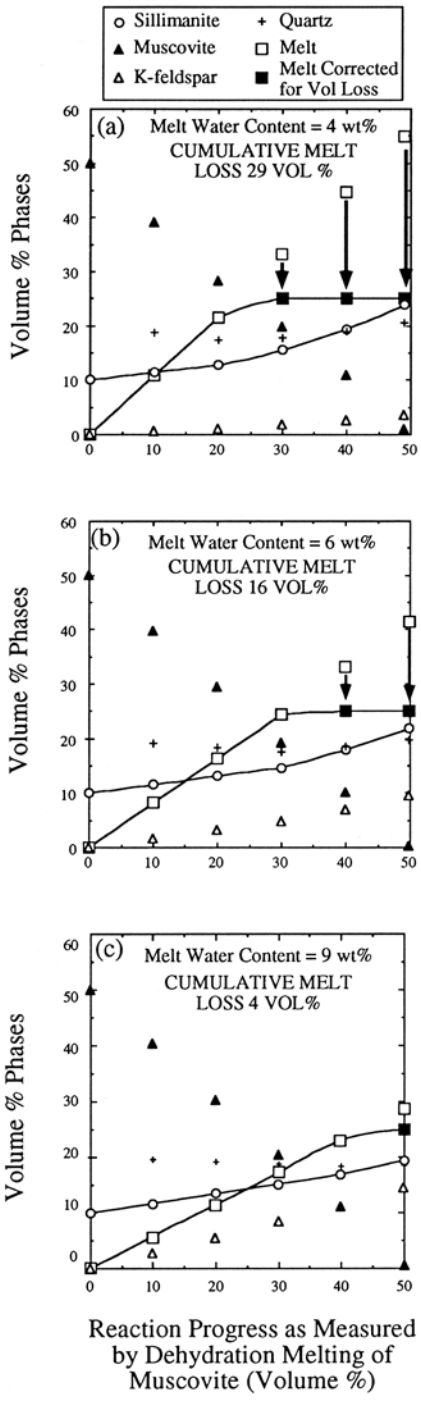

Fig. 9. Open-system behavior. Same as Fig. 8 except melt volumes >25 vol % are assumed lost from the system, resulting in a relative increase in the modal proportion of sillimanite and other phases. (a) Results using melt water content of 4 wt %; total melt production 54 vol %; cumulative melt loss 29 vol %. The resulting modal sillimanite volumes are approximately the same as those measured in the outcrop. (b) Results with a melt water content of 6 wt %; total melt production 41 vol %; cumulative melt loss 16 vol %. The volume of sillimanite is ~20%. (c) Results using a melt water content of 9 wt %; total melt production 29 vol %; cumulative melt loss 4 vol %. The volume of sillimanite is <20%.

mineral (Le Breton & Thompson, 1988). Melt volumes produced during vapor-absent melting of muscovite in the model pelite of this study are 54, 41, 29 and 24 total vol % for melt water contents of 4, 6, 9 and 12 wt %, respectively. These values far exceed any previous estimates of melt volume from the breakdown of muscovite. For muscovite vapor-absent melting, Clemens & Vielzeuf (1987) estimated 5–6 vol % melt, Miller (1985) reported 5–7 vol % and Le Breton & Thompson (1988) stated that melt volumes would be proportionally less than those produced from biotite vapor-absent melting (<20 vol %). These lower values are due to a combination of the lower modal proportion of muscovite in their protolith and generally higher water contents of the undersaturated melts assumed by these workers. For example, Clemens & Vielzeuf (1987) used a model pelite consisting of 0–10 wt % muscovite (0–28 modal %).

The high modal proportion of muscovite used in our modeling is justified by the high modal abundance of sillimanite observed in the mesosome. Unless >10 vol % sillimanite was produced at lower grade, or other high-grade reactions produced additional sillimanite, there must have been a large modal abundance of muscovite in the unmelted protolith, a conclusion consistent with measured mode of a lower-grade sample from nearby Mica Creek area. Notably, even with the large amount of muscovite in the metapelite, our modeling suggests that the observed modal proportion of sillimanite can never be produced in a closed system, even using an extreme melt water content of 12 wt % (Fig. 8d).

The assumed melt water content is the most important determinant of whether melt was lost from the system. Focusing on melt production alone, if melt water contents are in a range of 10–12 wt %, our modeling nearly reproduces the observed volume percent leucosome assuming closed-system melting. However, if values range between 4 and 9 wt % or less our modeling indicates that a larger volume of melt was produced, some of which must have been lost from the system. If calculations of melt water content using Burnham's model indeed overestimate the amount of water, melt water contents were probably ⩽9 wt %. The model of Nicholls indicates a much lower melt water content of ~4 wt %, using a melt composition similar to that of the leucosome. Two observations of the natural migmatites and results of our modeling support a low melt water content: (1) the apparent absence of solid K-feldspar in the mesosome is in contrast to model results that show volumetric production of solid K-feldspar for high melt water content; (2) the high modal percentage of sillimanite could only be reproduced assum-

ing low melt water contents and significant melt extraction. Consequently, we argue that a melt water content of between 4 and 6 wt% is most reasonable for the P–T conditions and composition of the leucosomes. From Fig. 9a and 9b, this indicates a melt loss of 16–29 vol% from a total melt production of 41–54 vol%. These results indicate that a muscovite-rich pelite can produce a substantial volume of melt from vapor-absent melting without fluid infiltration.

Melt extraction processes

Understanding processes of melt segregation and movement in the mid- and lower crust has important implications for the generation of migmatites as well as evaluation of the connection between migmatites and granites (Brown, 1994). Recent studies have focused on deformation-enhanced segregation processes such as fracture mechanisms facilitated by increasing pore pressure from the melt (Pattison & Harte, 1988; Harte *et al.*, 1991; Clemens & Mawer, 1992; Davidson *et al.*, 1994) and melt movement facilitated by shear zone deformation (Hollister & Crawford, 1986). Melt segregation may also be in part driven by buoyancy differences although, on the basis of mechanical and thermal considerations, whole-scale diapirism and convective overturn of melt-saturated rocks no longer appears to be a viable mechanism (Brown, 1994).

The modeling from this study indicates a melt volume loss of melt of 16–29% from a total melt production of 41–54 vol%. As the outcrop is not chaotically deformed (e.g. Pattison & Harte, 1988; Harte *et al.*, 1991), the accumulation of melt within the outcrop must not have reached a level to produce diatexites. The most likely explanation is that all of the melt was not produced at the same time and that during deformation a portion of the melt volume was removed (Pitcher, 1979; Clemens & Mawer, 1992).

There are several structures in the outcrop that are potential melt extraction pathways. Subvertical dikes at high angles to the foliation, 2–5 cm wide, are present throughout the outcrop (Fig. 3). This orientation is consistent with extension during flattening parallel to the subhorizontal fabric, which would provide subvertical fracture openings during deformation. The mineralogy and textures of the subvertical veins and dikes are indistinguishable from the foliation-parallel leucosomes and, where the layer-parallel and high-angle leucosomes intersect, there is a continuous textural transition between the two.

A ubiquitous feature throughout the outcrop is shear bands which deflect the foliation and deform leucosomes. Mesosome adjacent to well-developed shear bands is always depleted in K-feldspar. Some shear bands occasionally contain K-feldspar + quartz aggregates, whereas the adjacent rock is devoid of leucosome material, suggesting that melt may have migrated in response to a pressure gradient set up during shear band formation.

Finally, melt accumulated within the rock could escape when fracturing occurs in response to build-up of fluid pressure and decrease in the effective normal stress (Fig. 4c). If melt traveled in small portions during shear band formation it could leave the system along the foliation planes during continued deformation of the fabric. Although this process may only allow segregation and dispersion of small amounts of melt at any one time, repeated fracturing during deformation would permit larger amounts of melt to be extracted. Given the relative paucity of subvertical fractures compared with foliation-parallel leucosomes, this may be the most likely melt extraction process.

In a regional framework, the migmatite outcrop is close to the map trace of the Monashee décollement, a major thrust which displaced the Monashee Terrane eastward over the autochthonous and parautochthonous rocks of the North American craton (Brown & Carr, 1990). Melt-saturated rocks such as the studied outcrop and other nearby migmatized rocks in the vicinity of the décollement may have acted as a lubricant to facilitate and localize thrusting. Such melt-enhanced deformation has been described by Hollister & Crawford (1986). In turn, the pressure gradients induced thrusting may have facilitated escape of the melt.

ACKNOWLEDGEMENTS

Research for this work was conducted while M.W.N. was a Postdoctoral Fellow at The University of Calgary. Final preparation of the manuscript was completed while M.W.N. was a National Science Foundation postdoctoral fellow at the University of New Mexico. Research funds were supplied by a University of Calgary and, for final manuscript preparation, a National Science Foundation postdoctoral fellowship to M.W.N. and NSERC research grants to D.R.M.P. and E.D.G. Thorough and constructive reviews by John Clemens and Tom Foster were instrumental in clarifying several aspects of this work and are greatly appreciated.

REFERENCES

Ashworth, J. R., 1985. Introduction. In: Ashworth, J. R. (ed.) *Migmatites*. Glasgow: Blackie, pp. 1–35.

Ashworth, J. R. & McLellan, E., 1985. Textures. In: Ashworth, J. R. (ed.) *Migmatites*. Glasgow: Blackie, pp. 180–203.

Bence, A. E. & Albee, A. L., 1968. Empirical correction factors for the electron microanalysis of silicates and oxides. *Journal of Geology*, **76**, 382–403.

Berman, R. G., 1988. Internally-consistent thermodynamic data for stoichiometric minerals in the system Na_2O–K_2O–CaO–MgO–FeO–Fe_2O_3–Al_2O_3–SiO_2–TiO_2–H_2O–CO_2. *Journal of Petrology*, **29**, 445–522.

Berman, R. G., 1990. Mixing properties of Ca–Mg–Fe–Mn garnets. *American Mineralogist*, **75**, 328–344.

Berman, R. G., 1991. Thermobarometry using multiequilibrium calculations: a new technique with petrologic applications. *Canadian Mineralogist*, **29**, 833–855.

Billings, M. P., 1937. Regional metamorphism of the Littleton–Moosilauke area, N.H. *Geological Society of America Bulletin*, **48**, 463–565.

Brown, M., 1994. The generation, segregation, ascent and emplacement of granite magma: the migmatite-to-crustally-derived granite connection in thickened orogens. *Earth-Science Reviews*, **36**, 83–130.

Brown, R. L. & Carr, S. D., 1990. Lithospheric thickening and orogenic collapse within the Canadian Cordillera. In: Pacific Rim 90 Congress, Brisbane, Australia. *Journal of Australasian Institute of Mining and Metallurgy*, **2**, 1–10.

Burnham, C. W., 1979. The importance of volatile constituents. In: Yoder, H. S. (ed.) *The Evolution of the Igneous Rocks*. Princeton, NJ: Princeton University Press, pp. 439–482.

Chatterjee, N. M. & Johannes, W., 1974. Thermal stability and standard thermodynamic properties of synthetic $2M_1$-muscovite, $KAl_2[AlSi_3O_{10}](OH)_2$. *Contributions to Mineralogy and Petrology*, **48**, 89–114.

Chinner, 1960. Pelitic gneisses with varying ferrous/ferric ratios from Glen Cova, Angus, Scotland. *Journal of Petrology*, **1**, 178–217.

Clemens, J. D., 1984. Water contents of silicic to intermediate magmas. *Lithos*, **17**, 273–287.

Clemens, J. D. & Mawer, C. K., 1992. Granitic magma transport by fracture propagation. *Tectonophysics*, **204**, 339–360.

Clemens, J. D. & Vielzeuf, D., 1987. Constraints on melting and magma production in the crust. *Earth and Planetary Science Letters*, **86**, 287–306.

Clemens, J. D. & Wall, V. J., 1981. Origin and crystallization of some peraluminous (S-type) granitic magmas. *Canadian Mineralogist*, **19**, 111–131.

Davidson, C., Schmid, S. M. & Hollister, L. C., 1994. Role of melt during deformation in the deep crust. *Terra Nova*, **6**, 133–142.

Dougan, T. W., 1979. Compositional and modal relationships and melting relationships in some migmatitic metapelites from New Hampshire and Maine. *American Journal of Science*, **279**, 897–935.

Dougan, T. W., 1981. Melting reactions and trace element relationships in selected samples of migmatitic pelites from Maine and New Hampshire. *Contributions to Mineralogy and Petrology*, **78**, 337–344.

Foster, C. T., Jr, 1977. Mass transfer in sillimanite-bearing pelitic schist near Rangeley, Maine. *American Mineralogist*, **62**, 727–764.

Fuhrman, M. L. & Lindsley, D. H., 1988. Ternary-feldspar modeling and thermometry. *American Mineralogist*, **73**, 201–216.

Ghent, E., 1975. Temperature, pressure, and mixed-volatile equilibria attending metamorphism of staurolite–kyanite-bearing assemblages, Esplanade Range, British Columbia. *Geological Society of America Bulletin*, **86**, 1654–1660.

Greenwood, H. J., Woodsworth, G. J., Read, P. B., Ghent, E. D. & Evenchick, C. A., 1991. Metamorphism. In: Gabrielse, H. & Yorath, C. J. (eds), *Geology of the Cordilleran Orogen in Canada. Geology of Canada*, **4**. Ottawa: Geological Survey of Canada, pp. 533–570.

Guidotti, C. V., 1970. The mineralogy and petrology of the transition zone from the lower to upper sillimanite zone in the Oquossoc area, Maine. *Journal of Petrology*, **11**, 277–366.

Harte, B., Pattison, D. R. M. & Linklater, C. M., 1991. Field relations and petrography of partially melted pelitic and semipelitic rocks. In: Voll, G., Topel, J., Pattison, D. R. M. & Seifert, F. (eds) *Equilibrium and Kinetics in Contact Metamorphism*. Berlin: Springer-Verlag, pp. 183–209.

Hollister, L. S. & Crawford, M. L., 1986. Melt-enhanced deformation: a new tectonic process. *Geology*, **14**, 558–561.

Kenah, C. & Hollister, L. S., 1983. Anatexis in the Central Gneiss Complex, British Columbia. In: Atherton, M. P. & Gribble, C. D. (eds) *Migmatites, Melting and Metamorphism*. Nantwich, Cheshire: Shiva, pp. 142–162.

Klein, C. & Hurlburt, C. S., Jr, 1993. *Manual of Mineralogy*. New York: John Wiley.

Kretz, R., 1983. Symbols for rock-forming minerals. *American Mineralogist*, **68**, 277–279.

Le Breton, N. & Thompson, A. B., 1988. Fluid-absent (dehydration) melting of biotite in metapelites in the early stages of crustal anatexis. *Contributions to Mineralogy and Petrology*, **99**, 226–237.

McLellan, E. L., 1985. Metamorphic reactions in the kyanite and sillimanite zones of the Barrovian type area. *Journal of Petrology*, **26**, 789–818.

McMullin, D., Berman, R. G. & Greenwood, H. J., 1991. Calibration of the SGAM thermobarometer for pelitic rocks using data from phase equilibrium experiments and natural assemblages. *Canadian Mineralogist*, **29**, 889–908.

Mehnert, D. R., 1968. *Migmatites and the Origin of Granitic Rocks*. Amsterdam: Elsevier.

Miller, C. F., 1985. Are strongly peraluminous magmas derived from pelitic sedimentary sources? *Journal of Geology*, **93**, 673–689.

Navrotsky, A., 1987. Calorimetric studies of melts, crystals, and glasses, especially in hydrous systems. In: Mysen, B. O. (ed.) *Magmatic Processes: Physiochemical Principles. Geochemical Society Special Publication*, **1**, 411–422.

Nicholls, J., 1980. A simple thermodynamic model for estimating the solubility of H_2O in magmas. *Contributions to Mineralogy and Petrology*, **74**, 211–220.

Nicholls, J., Fiesinger, D. & Ethier, V. G., 1977. FORTRAN IV programs for processing routine electron microprobe data. *Computers in Geosciences*, **3**, 49–83.

Nicholls, J. & Stout, M. Z., 1988. Picritic melts in Kilauea—evidence from the 1967–1968 Halemaumau and Kiiada eruptions. *Journal of Petrology*, **29**, 1031–1057.

Novak, J. M. & Holdaway, M. J., 1981. Metamorphic petrology, mineral equilibria, and polymetamorphism in the Augusta Quadrangle, south-central Maine. *American Mineralogist*, **66**, 51–69.

Olsen, S., 1982. Open- and closed-system migmatites in the Front Range, Colorado. *American Journal of Science*, **282**, 1596–1622.

Olsen, S., 1984. Mass-balance and mass-transfer in migmatites from the Colorado Front Range. *Contributions to Mineralogy and Petrology*, **85**, 30–44.

Pattison, D. R. M. & Harte, B., 1988. Evolution of structurally contrasting anatectic migmatites in the 3-kbar Ballachulish aureole, Scotland. *Journal of Metamorphic Geology*, **6**, 475–494.

Peterson, J. W. & Newton, R. C., 1989. Reversed experiments on biotite–quartz–feldspar melting in the KMASH: implications for crustal anatexis. *Journal of Geology*, **92**, 465–485.

Peto, P., 1976. An experimental investigation of melting relations involving muscovite and paragonite in the silica-saturated portion of the system K_2O–Na_2O–Al_2O_3–SiO_2–H_2O to 15 kb total pressure. *Progress in Experimental Petrology. 3rd Report*. London: NERC, pp. 41–45.

Pitcher, W. S., 1979. The nature, ascent and emplacement of granitic magmas. *Journal of the Geological Society, London*, **136**, 627–662.

Raeside, R. P., 1982. Structure, metamorphism and migmatization of Scripp Range, Mica Creek, B.C. Unpublished Ph.D. Thesis, University of Calgary, Calgary, Alberta, 204 pp.

Robbins, D. B., 1976. Metamorphism and structure of Encampment Creek area, B.C. Unpublished M.Sc. Thesis, University of Calgary, Calgary, Alberta, 171 pp.

Scammell, R. J. & Brown, R. L., 1990. Cover gneisses of the Monashee Terrane: a record of synsedimentary rifting in the North American Cordillera. *Canadian Journal of Earth Sciences*, **27**, 712–726.

Spear, F. S. & Cheney, J. T., 1989. A petrogenetic grid for pelitic schists in the system SiO_2–Al_2O_3–FeO–MgO–K_2O–H_2O. *Contributions to Mineralogy and Petrology*, **101**, 149–164.

Stolper, E., 1982. Water in silicate glasses: an infrared spectroscopic study. *Contributions to Mineralogy and Petrology*, **81**, 1–17.

Större, B., 1972. Dry melting of muscovite + quartz in the range P_S=7 kb to P_S=20 kb. *Contributions to Mineralogy and Petrology*, **37**, 87–89.

Thompson, A. B., 1983. Fluid-absent metamorphism. *Journal of the Geological Society, London*, **140**, 533–547.

Thompson, A. B. & Algor, J. R., 1977. Model systems for anatexis of pelitic rocks I. Facies series melting and reactions in the system $KAlO_2$–$NaAlO_2$–Al_2O_3–SiO_2–H_2O. *Contributions to Mineralogy and Petrology*, **63**, 247–269.

Thompson, A. B. & Tracy, R. J., 1979. Model systems for anatexis of pelitic rocks II. Facies series melting and reactions in the system CaO–$KAlO_2$–$NaAlO_2$–Al_2O_3–SiO_2–H_2O. *Contributions to Mineralogy and Petrology* **70**, 429–438.

Tracy, R. J., 1982. Compositional zoning and inclusions in metamorphic minerals: In: Ferry, J. M. (ed.) *Characterization of Metamorphism through Mineral Equilibria. Mineralogical Society of America Reviews in Mineralogy*, **10**, 355–397.

Tracy, R. J., 1986. Modelling the residuum from formation and extraction of partial melts in pelites. *Geological Society of America Abstracts with Programs*, **18**, 775.

Vernon, R. H. & Collins, W. J., 1988. Igneous microstructures in migmatites. *Geology*, **16**, 1126–1129.

Vielzeuf, D. & Clemens, J. D., 1992. The fluid-absent melting of phlogopite + quartz: experiments and models. *American Mineralogist*, **77**, 1206–1222.

Vielzeuf, D. & Holloway, J. R., 1988. Experimental determination of the fluid-absent melting relations in the pelitic system: consequences for crustal differentiation. *Contributions to Mineralogy and Petrology*, **98**, 257–276.

Waters, D. J., 1988. Partial melting and the formation of granulite facies assemblages in Namaqualand, South Africa. *Journal of Metamorphic Geology*, **6**, 387–404.

Yardley, B. W. D., 1978. Genesis of the Skagit Gneiss migmatites, Washington, and the distinction between possible mechanisms of migmatization. *Geological Society of America Bulletin*, **89**, 941–951.

RECEIVED OCTOBER 15, 1993
REVISED TYPESCRIPT ACCEPTED JULY 11, 1994

APPENDIX: MODELING METHODS AND PARAMETERS

Volume changes associated with staurolite-out reaction

To constrain the amount of Al-silicate that may have been contained in the pelites before muscovite vapor-absent melting, modal amounts of staurolite and Al-silicates for pelites at or slightly above the staurolite-out reaction were compiled in Table A1. Calculations of volume changes of the different phases during staurolite breakdown were calculated. The compositions of the phases in Table A2 were taken from Ghent (1975) for pelites at staurolite grade conditions in the nearby Mica Creek area. Changes in the mineral abundances shown in Fig. 8 were calculated using the reaction coefficients, molecular weights and densities listed in Table A2. It is assumed that any kyanite formed before or during staurolite breakdown was converted to sillimanite at the kyanite–sillimanite transition.

Table A1: Modal estimates of kyanite or sillimanite and staurolite from lower to upper sillimanite zones

Reference	Location	Metamorphic conditions	Av. modal St and SD	Av. modal Sil/Ky and SD
Billings (1937)	Moosilauke, NH, USA	Lower sillimanite zone	3	Sil: 7
Chinner (1960)	Glen Cova, Scotland	Lower sillimanite zone	0·3 (0·7)	Si: 8·7 (12·8)
Guidotti (1970)	Oquossoc, ME, USA	575–630°C; 3–5 kbar	8·0 (6·3)	Sil: tr
Novak & Holdaway (1981)	Augusta, ME, USA	530–610°C; 2·8–4·8 kbar	3·0 (3·2)	Sil: 2·2 (5·5)
Robbins (1976)*	Mica Creek area, B.C., Canada	635–641°C; 7–9 kbar	4·0 (3·5)	Ky: 5
Foster (1977)	Rangley, ME, USA	650°C; 5 kbar	4·9 (4·1)	Sil: 1·6 (1·0)
Raeside (1982)*	Mica Creek area, B.C., Canada	600–700°C; 6–7 kbar	—	Ky: 5·0 (2·0)
McLellan (1985)	Grampian Mtns, Scotland	550–650°C; 6 kbar	5·6 (4·4)	—

*Hand specimens and thin sections examined from these areas.

Table A2: Cations, gram formula weight (GFW), densities of phases and reaction coefficients used in volume calculations for St-out reaction

	Ms	Qtz	St	Sil	Bt	Grt	Water
K	0·89	0·00	0·00	0·00	0·82	0·00	0·00
Fe	0·00	0·00	2·92	0·00	1·12	1·97	0·00
Mg	0·12	0·00	0·68	0·00	1·33	0·14	0·00
Al	2·89	0·00	17·20	2·00	1·69	1·96	0·00
Si	3·04	1·00	7·33	1·00	2·71	2·98	0·00
O	11	2	44	5	11	12	1
H	2	0	4	0	2	0	2
GFW (g/mol)	387·14	60·09	1620	162·05	442·55	441·90	18·00
Density (g/cm^3)	2·82	2·65	3·70	3·23	3·0	3·8	—
Reaction coeff.	0·065	0·481	0·129	−1·00	−0·055	−0·160	−0·268

Negative values for reaction coefficients indicate products; positive values are reactants. Densities from Klein & Hurlburt (1993).

Table A3: Cations, gram formula weight (GFW) and density of phases used in volume calculations for Ms-dehydration melting reaction

	Ms	Kfs	Sil	Qtz	Melt	Melt	Melt	Melt
K	0·71	0·81	0	0	0·55	0·58	0·58	0·58
Al	2·95	0·95	2	0	0·65	0·67	0·67	0·67
Si	3·11	3·09	1	1	4·37	4·35	4·35	4·35
O	11	8	5	2	10	10	10	10
wt%	4·23	—	—	—	4	6	9	12
H_2O								
GFW (g/mol)	370·84	272·02	162·05	60·09	321·93	323·16	323·45	323·64
Density (g/cm^3)	2·82	2·57	3·23	2·65	2·2	2·2	2·2	2·2

Densities of silicate phases are from Klein & Hurlburt (1993). Density of melt is from Clemens & Vielzeuf (1987). Melt cations were calculated on anhydrous basis of 10 oxygens. For each melt composition, the weight percent was renormalized to 100 for the different water contents. The total GFW of the melt was calculated by adding the weight of the anhydrous component and the GFW of water for each melt composition.

Table A4: Reaction coefficients for Ms-dehydration melting with various melt water contents in the system K_2O–Al_2O_3–SiO_2–H_2O

	Ms	Qtz	Kfs	Sil	Melt
$XH_2O = 4·0$	1	0·51	−0·07	−0·44	−1·0
$XH_2O = 6·0$	1	0·39	−0·20	−0·44	−0·74
$XH_2O = 9·0$	1	0·29	−0·34	−0·44	−0·51
$XH_2O = 12·0$	1	0·24	−0·41	−0·44	−0·39

Negative values indicate products of reaction, positive values are reactants.